NANO LETTERS

pubs.acs.org/NanoLett

Supported Ru−Pt Bimetallic Nanoparticle Catalysts Prepared by Atomic Layer Deposition

Steven T. Christensen,[†] Hao Feng,[†] Joseph L. Libera,[†] Neng Guo,[†] Jeffrey T. Miller,[†] Peter C. Stair,[†,‡] and Jeffrey W. Elam*[,†]

[†]Argonne National Laboratory, Argonne, Illinois 60439 and [‡]Department of Chemistry, Northwestern University, Evanston, Illinois 60208

ABSTRACT Atomic layer deposition (ALD) is used to deposit ruthenium−platinum nanostructured catalysts using 2,4-(dimethylpentadienyl)(ethylcyclopentadienyl) ruthenium, trimethyl(methylcyclopentadienyl) platinum, and oxygen as precursors. Transmission electron microscopy shows discrete 1.2 nm nanoparticles decorating the surface of the spherical alumina support. The Ru−Pt particles are crystalline and have a crystal structure similar to pure platinum. X-ray fluorescence measurements show that the nanoparticle composition is controlled by the ratio of metal precursor ALD cycles. X-ray absorption spectroscopy at the Ru K-edge indicates a nearest neighbor Ru−Pt interaction consistent with a bimetallic composition. Methanol decomposition reactions further confirm a Ru−Pt interaction and show enhanced methanol conversion for the bimetallic nanoparticles when compared to catalysts comprised of a mixture of pure Pt and Ru nanoparticles of similar loading. These results demonstrate that ALD is a viable technique for synthesizing mixed-metal nanostructures suitable for catalysis and other applications.

KEYWORDS Atomic layer deposition, platinum, ruthenium, bimetallic catalysts

Atomic layer deposition (ALD) is a thin film growth technique that employs self-limiting chemical reactions between gaseous precursors and a solid surface allowing atomic scale control over the film thickness and composition.[1,2] One of the distinguishing attributes of ALD is the capability to deposit highly uniform and conformal coatings on surfaces with complex topographies and to infiltrate mesoporous materials.[3−5] This feature is particularly attractive for the synthesis of heterogeneous catalysts requiring highly dispersed catalytic species on high surface area, mesoporous supports. Consequently, ALD is being explored as an alternative method for preparing advanced catalysts.[6−9]

The layer-by-layer growth process afforded by ALD typically yields smooth, uniform films and this is ideal for most microelectronics applications.[10] However, nonuniform deposits can result when the ALD chemistry is inhibited on the starting substrate or when the ALD material aggregates from surface diffusion. Both of these mechanisms are in effect in the early stages of noble metal ALD on oxide surfaces resulting in the formation of discrete, three-dimensional nanoparticles that decorate the surface.[11−15] This behavior has been exploited to synthesize supported noble metal catalysts exhibiting remarkably high activity as a result of the highly dispersed, small noble metal particles.[9,16−18]

Historically, noble metal ALD has been limited to single-component films[11,19−23] but very recently the ALD of mixed-metal films has been reported.[24,25] This capability could provide enormous technological benefit if the method could be broadened to include a range of other mixed-metal combinations and particularly if the technique could be extended to synthesize mixed-metal nanoparticles. Mixed-noble metal nanoparticles can exhibit superior catalytic properties[26] compared to both their single-component counterparts as well as their thin film analogs resulting in higher conversions and lower required loadings of the costly precious metals. This is especially true for the ruthenium−platinum catalysts used in direct methanol fuel cells (DMFCs) where a bimetallic catalyst is required for optimal performance.[27,28] In our previous work on the ALD of Ir−Pt films, we found that the films deposit as alloys in which the composition and properties obey rule of mixtures formulas. Such predictable behavior suggests that this method might apply to other ALD mixed-noble metal combinations that share compatible surface chemistries. However, the formation of bimetallic nanoparticles may be complicated by additional factors including the interaction of the underlying support surface and the relative rates of nucleation and growth for the different metal components.

In this communication, we report on the ALD of Ru−Pt bimetallic nanoparticles. These metals were selected based on their importance as fuel cell catalysts and on their similar ALD chemistries and growth conditions. First, we utilize in situ quartz crystal microbalance (QCM) measurements to verify growth of the mixed-metals under our conditions.

* To whom correspondence should be addressed. E-mail: jelam@anl.gov.
Received for review: 05/3/2010
Published on Web: 07/12/2010

DOI: 10.1021/nl101567m | *Nano Lett.* **2010,** *10,* 3047–3051

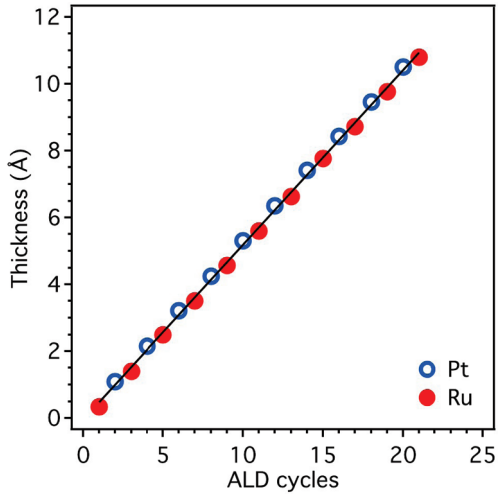

FIGURE 1. In situ QCM measurements performed during Ru−Pt mixed-metal ALD using a 1:1 ratio of Ru(DER) to Pt(MeCp)Me$_3$ cycles.

Next, we prepare Ru−Pt mixed-metal deposits on spherical alumina nanoparticles and characterize the materials using transmission electron microscopy (TEM) to determine the morphology of the Ru−Pt deposits and verify the existence of nanoparticles. We also utilize X-ray fluorescence (XRF) to evaluate the composition (Ru and Pt mol %) and the metal loading and utilize extended X-ray absorption fine structure spectroscopy (EXAFS) to examine the structure. The EXAFS measurements probe the degree of interaction between the platinum and ruthenium atoms and can positively identify bimetallic nanoparticles. Finally, we test the resulting materials for their catalytic behavior using methanol decomposition, the initial reaction in DMFCs. The catalytic behavior provides an additional probe of the interaction between Ru and Pt when compared to the behavior of the monometallic components.

ALD was performed using alternating exposures to 2,4-(dimethylpentadienyl)(ethylcyclopentadienyl) ruthenium (Ru(DER)) and oxygen for Ru ALD[23] and trimethyl(methylcyclopentadienyl) platinum (Pt(MeCp)Me$_3$) and oxygen for Pt ALD.[21] By adjusting the ratio between the Ru(DER)/O$_2$ cycles and the Pt(MeCp)Me$_3$/O$_2$ cycles, we should in principle control precisely the Ru/Pt ratio in the deposits. To confirm this hypothesis, we used in situ QCM measurements to monitor the thickness changes during Ru−Pt mixed-metal ALD using a 1:1 ratio of Ru(DER) to Pt(MeCp)Me$_3$ cycles. Figure 1 demonstrates linear growth with reproducible thickness increments of 0.31 ± 0.02 Å/cycle during each Ru ALD cycle and 0.74 ± 0.03 Å/cycle during each Pt ALD cycle assuming bulk Pt and Ru densities. These values are very similar to the growth rates we measured by QCM for the pure Ru and Pt ALD indicating very little perturbation of the growth chemistries upon transitioning between materials. Consequently, our QCM measurements confirm that we can control the Ru/Pt ratio in a similar fashion as Ir−Pt ALD alloys.[24] Furthermore, these measurements indicate that 2−3 Ru ALD cycles should be performed for each Pt ALD cycle to achieve approximately equal amounts (mol %) of these metals in the deposit.

We next prepared ALD Ru−Pt on spherical Al$_2$O$_3$ powder using the following scheme: 2 cycles Ru(DER)/O$_2$; 1 cycle Pt(MeCp)Me$_3$/O$_2$; and 1 cycle Ru(DER)/O$_2$. This Ru−Ru−Pt−Ru ALD sequence yielded a metal loading of 4 wt % as measured from mass uptake. The noble metal composition was determined by XRF to be 71 mol % Ru. This value is somewhat higher than the predicted value of 58 mol % Ru based on the relative ALD growth rates and the number of cycles performed, and this divergence probably results from differences in the chemisorption of the metal precursors on the Al$_2$O$_3$ surface as compared to the noble metal surface. We also observed that the order in which the Pt ALD and Ru ALD cycles are performed affects slightly the composition. A more detailed investigation is under way to explore these phenomena.

Figure 2a shows a TEM micrograph of a typical 40−60 nm diameter Al$_2$O$_3$ nanosphere following the Ru−Ru−Pt−Ru ALD sequence and clearly shows that the Ru−Pt deposit consists of isolated nanoparticles. The inset in Figure 2a shows a histogram of particle sizes measured from the TEM image and yields an average particle size of 1.2 ± 0.3 nm. This particle size is consistent with the size of ALD Pt nanoparticles prepared on strontium titanate surfaces under similar conditions.[14] Figure 2b shows a high-resolution micrograph where lattice fringes for both the Al$_2$O$_3$ and the metal nanoparticles are visible. The lattice fringes for the Al$_2$O$_3$ are approximately 0.47 nm and are consistent with the d-spacing for Al$_2$O$_3$ (100) planes of 0.48 nm. The nanoparticles show lattice fringes of ~0.19 nm. The d-spacing for the (200) lattice planes in Pt is 0.19 nm whereas the (101) planes in Ru are spaced at 0.21 nm. Our TEM images do not provide sufficient resolution to quantify the changes in crystal structure expected for Ru−Pt bimetallic nanoparticles. However, the TEM images show that the metal nanoparticles are crystalline and faceted and appear to assume a structure similar to bulk Pt.

To differentiate between separate Ru and Pt particles versus bimetallic Ru−Pt particles, EXAFS measurements of the Ru−Pt were performed. Figure 3a shows the Ru K-edge X-ray absorption near edge structure (XANES) spectra of the Ru−Pt ALD/alumina bimetallic catalysts and that of a 3% Ru/silica catalyst with 5 nm metallic nanoparticles. The bimetallic Ru−Pt XANES is shifted to higher energy by ~3 eV, and the shape of the edge and of the first two peaks are significantly different, indicating that this is not Ru only. Figure 3b shows the magnitude and the imaginary parts of Fourier transform of the Ru K-edge EXAFS for these two catalysts. The magnitude of the Fourier transform for the first shell coordination of Ru/silica has two peaks, one large peak at about 2.5 Å and a smaller peak at about 2 Å. This spectrum is typical of the K-edge EXAFS for a single 4d metal. The magnitude of the Fourier transform of the Ru−Pt

DOI: 10.1021/nl101567m | *Nano Lett.* **2010,** *10,* 3047–3051

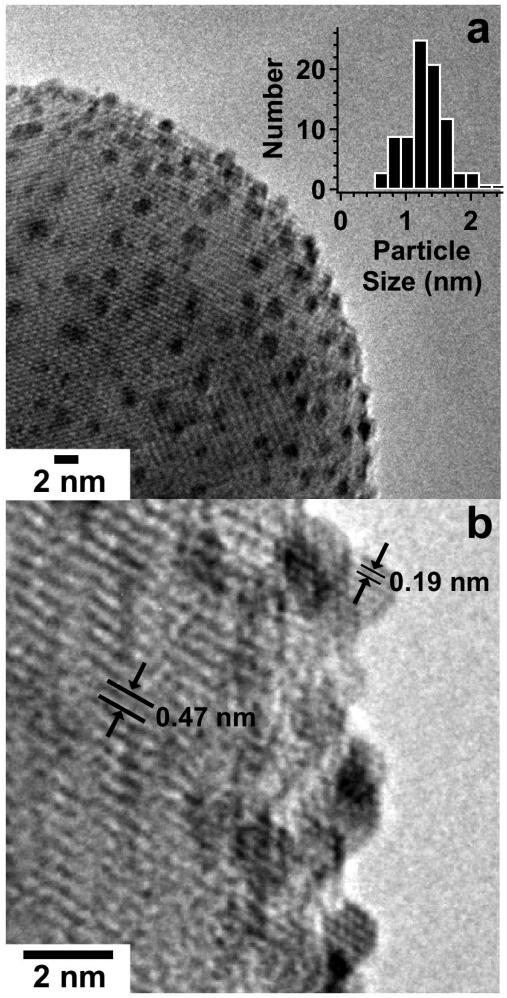

FIGURE 2. TEM images of ALD nanoparticles on Al_2O_3. (a) ALD metal nanoparticles decorate the alumina sphere. The histogram gives the nanoparticle size distribution measured from TEM where the mean particle diameter is 1.2 nm with a distribution width of 0.3 nm. (b) High-resolution TEM image showing lattice fringes for the Al_2O_3 and the Ru−Pt nanoparticles.

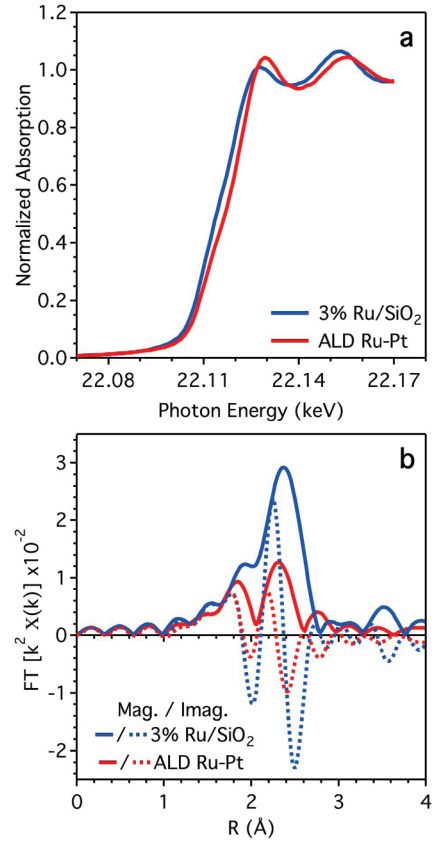

FIGURE 3. X-ray absorption data. (a) Ru K-edge spectra for ALD Ru−Pt/Al_2O_3 and a reference 3% Ru/SiO_2. For the ALD catalysts, the Ru K-edge is shifted 3 eV higher and has a distinctly different line profile compared to the Ru reference. (b) Fourier transforms (Δk = 2.7−12.2 $Å^{-1}$) of the absorption spectra where the solid line shows the magnitude and the broken line shows the imaginary part. Peaks at 2 and 2.5 Å are smaller for the ALD catalyst when compared to the Ru reference. Fitting this data to a Ru−Pt bimetallic model provides the data in Table 1.

TABLE 1. Ru K-edge EXAFS Fitting Results

scatter	N (±20%)	R (±0.02 Å)	$\Delta\sigma^2$ $Å^2$ (x 10^3)	E_o (eV)
Ru−Ru	3.8	2.60	2.0	−3.0
Ru−Pt	4.5	2.69	2.0	−5.0

alloy also has two peaks, but the intensity of the smaller peak is nearly equivalent to that of the second indicating the presence of a second metal scatterer, that is, Ru−Ru and Ru−Pt. Fitting both the magnitude and imaginary parts of the Fourier transform to a model that includes Ru and Pt enables us to extract bond distances for Ru−Ru and Ru−Pt as well as the coordination numbers, N. These data are given in Table 1 along with the other fitting parameters. The Ru−Ru bond distance is 2.60 Å, which is significantly shorter than that in Ru foil, 2.68 Å. The Ru−Pt bulk bond distance is 2.72 Å while that in the Ru−Pt catalyst is 2.69 Å. These bonding results provide further evidence of a Ru−Pt interaction, and the contraction of the bond distances is consistent with small metallic particles.[15,29]

Figure 4 shows the methanol conversion as a function of temperature for the bimetallic Ru−Pt catalyst and a physical mixture of ALD Pt on spherical alumina and ALD Ru on spherical alumina. The Ru−Pt bimetallic catalyst shows a higher CH_3OH conversion than the single mixture at temperatures above 210 °C. Furthermore, the CH_3OH conversion for the bimetallic catalyst begins to saturate at 250 °C, while the physical mixture does not appear to saturate even at 270 °C. The steeper temperature dependence implies a higher activation energy for the bimetallic catalyst as compared to the physical mixture and supports that the Ru−Pt mixed metal ALD yields bimetallic nanoparticles.

In conclusion, ALD offers a broad set of tools to construct very small, supported bimetallic nanostructures for application in fuel cells or heterogeneous catalysis. This initial study focused on Ru−Pt mixed metal ALD using established ruthenium and platinum ALD chemistries. TEM reveals that the Ru−Pt deposits as discrete nanoparticles with a diameter of 1.2 nm on the alumina support, and EXAFS measure-

DOI: 10.1021/nl101567m | Nano Lett. 2010, 10, 3047--3051

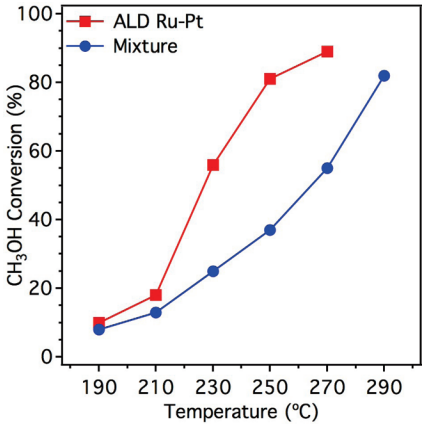

FIGURE 4. Methanol decomposition as a function of temperature for the Ru−Pt bimetallic catalyst and the physical mixture of Ru + Pt monometallic catalysts. The Ru−Pt bimetallic shows a higher CH_3OH conversion above 210 °C.

ments confirm that the Ru−Pt nanoparticles are bimetallic. The Ru−Pt mixed metal ALD catalysts yield a higher conversion in the CH_3OH decomposition reaction compared to a physical mixture of monometallic Ru and Pt catalysts and this difference is further evidence that the Ru−Pt mixed metal ALD yields bimetallics. These results are particularly encouraging for the development of multicomponent catalysts by ALD precursors. In future studies, we will elaborate on the ALD Ru−Pt bimetallic system and extend this method to other mixed-metal ALD processes and also perform more extensive characterization to elucidate the inner structure of the multimetallic nanoparticles.

Experimental Section. ALD was performed in a hot-walled viscous flow reactor equipped with an in situ quartz crystal microbalance (QCM) described elsewhere.[30] Aluminum oxide nanospheres (NanoDur, Alfa Aesar) with a diameter range of 40−60 nm and a surface area of ca. 35 m^2/g in quantities of ∼0.15 g were loaded into a stainless steel tray with a mesh top to contain the powder.[5] The tray was installed into the reactor at 300 °C, which was evacuated to 1 Torr under a continuous 240 sccm flow of ultrahigh purity nitrogen carrier gas. The ALD noble metal precursors were held in separate heated, stainless steel bubblers with the Pt(MeCp)Me_3 (Strem Chemicals, Inc.) at 50 °C and the Ru(DER) (Tosoh Corp.) at 80 °C. An exposure time of 200 s was used for the noble metal precursors and oxygen and 50 s purge periods were introduced between precursor exposures. TEM images were collected on a JEOL 3010 instrument operating at 300 keV.

Ru K-edge XAFS were performed at the Materials Research Collaborative Access Team (MRCAT) and CMC beamlines at the Advanced Photon Source, Argonne National Laboratory. The setup used was similar to that outlined by Castagnola et al.[31] The sample was loaded as a self-supporting wafer without binder in the channels (i.d. = 4 mm) of a stainless steel multisample holder. The sample holder was then placed in the center of a quartz tube, which was equipped with gas and thermocouple ports and Kapton windows. The amount of sample used was optimized for a step height of about 0.5. Prior to the XAFS measurements, the sample was reduced in 4% H_2/He at 300 °C for 30 min followed by He purge for 10 min. Next, the sample was cooled to RT in flowing He. The XAFS spectra were recorded in transmission mode. Standard procedures based on WINXAS 3.1 software were used to fit the XAS data. The EXAFS coordination parameters were obtained by a least-squares fit in q- and r-space of the isolated nearest neighbor, k^2-weighted Fourier transform data.

The catalytic experiments were carried out in a stainless-steel, microflow reactor with an inside diameter of ∼4 mm. Prior to performing the measurements, the reactor was passivated by coating with 50 nm of ALD Al_2O_3 to reduce interference from background reactions. Ten milligrams of catalyst were used in each experiment. The catalyst was held in the middle of the reactor by a plug of quartz wool. The catalyst mixture comprised Al_2O_3 nanospheres coated with either ALD Pt (5 wt % Pt) or ALD Ru (∼1 wt % Ru). The ALD Pt/alumia also has 1−2 nm Pt particles whereas the ALD Ru is less well-defined. The mixture was prepared by incrementally adding powder and measuring XRF until a 76 mol % Ru was obtained. A K-type thermocouple was positioned inside the reactor in contact with the catalyst layer to measure the reaction temperature. Methanol vapor was introduced into the reaction system using an argon (Airgas, 99.99%) gas bubbler. The bubbler was immersed in an ice−water bath to generate an argon stream with ∼4% methanol. Pure argon was used as the balance gas. The catalytic experiments were performed in the temperature range of 190 to 290 °C with a gas flow rate of 10 sccm at atmospheric pressure. The reactor was allowed to equilibrate for 0.5 h at each data point; each data point represents a 5 h duration in which the catalyst did not show any appreciable degradation in activity. The alloy catalyst was tested twice and good reproducibility was achieved. Reaction products were analyzed by an online HP 5890 gas chromatograph equipped with a thermal conductivity detector (TCD). Signals from the TCD were calibrated using certified standard gas mixtures (Scotty, 1.00% CO_2, 0.999% CO, 1.00% H_2, 0.998% CH_4, balance of nitrogen).

Acknowledgment. This work was supported by the U.S. Department of Energy, Office of Energy Efficiency and Renewable Energy, Industrial Technologies Program under contract YN-19-01-000. X-ray absorption measurements were performed at the insertion-device beamline of the Materials Research Collaborative Access Team (MR-CAT) at the Advanced Photon Source located within the Argonne National Laboratory. Use of the APS was supported by the U.S. Department of Energy, Office of Science, Office of Basic Energy Sciences, under Contract No. DE-AC02-06CH11357 operated by UChicago Argonne, LLC. MRCAT operations are supported by the Department of Energy and the MRCAT member institutions.

DOI: 10.1021/nl101567m | *Nano Lett.* **2010,** *10,* 3047--3051

REFERENCES AND NOTES

(1) Ritala, M.; Leskela, M. Atomic Layer Deposition. In *Handbook of Thin Film Materials*; Nalwa, H. S., Ed.; Academic Press: San Diego, 2001; Vol. 1, p 103.

(2) George, S. M. Atomic Layer Deposition: An Overview. *Chem. Rev.* **2010**, *110* (1), 111–131.

(3) Elam, J. W.; Routkevitch, D.; Mardilovich, P. P.; George, S. M. Conformal coating on ultrahigh-aspect-ratio nanopores of anodic alumina by atomic layer deposition. *Chem. Mater.* **2003**, *15* (18), 3507–3517.

(4) Elam, J. W.; Libera, J. A.; Pellin, M. J.; Zinovev, A. V.; Greene, J. P.; Nolen, J. A. Atomic layer deposition of W on nanoporous carbon aerogels. *Appl. Phys. Lett.* **2006**, *89* (5), 053124-1−053124-3.

(5) Libera, J. A.; Elam, J. W.; Pellin, M. J. Conformal ZnO coatings on high surface area silica gel using atomic layer deposition. *Thin Solid Films* **2008**, *516* (18), 6158–6166.

(6) Haukka, S.; Lakomaa, E. L.; Suntola, T. Adsorption controlled preparation of heterogeneous catalysts. In *Adsorption and Its Applications in Industry and Environmental Protection, Vol I: Applications in Industry*; Dabrowski, A., Ed.; Elsevier: New York, 1999; Vol. 120, pp 715−750.

(7) Stair, P. C.; Marshall, C.; Xiong, G.; Feng, H.; Pellin, M. J.; Elam, J. W.; Curtiss, L.; Iton, L.; Kung, H.; Kung, M.; Wang, H. H. Novel, uniform nanostructured catalytic membranes. *Top. Catal.* **2006**, *39* (3−4), 181–186.

(8) Pellin, M. J.; Stair, P. C.; Xiong, G.; Elam, J. W.; Birrell, J.; Curtiss, L.; George, S. M.; Han, C. Y.; Iton, L.; Kung, H.; Kung, M.; Wang, H. H. Mesoporous catalytic membranes: Synthetic control of pore size and wall composition. *Catal. Lett.* **2005**, *102* (3−4), 127–130.

(9) Lu, J.; Stair, P. C. Low-temperature ABC-type atomic layer deposition: Synthesis of highly uniform ultrafine supported metal nanoparticles. *Angew. Chem., Int. Ed.* **2010**, *49* (14), 2547–2551.

(10) Lee, F.; Marcus, S.; Shero, E.; Wilk, G.; Swerts, J.; Maes, J. W.; Blomberg, T. In *Atomic layer deposition: An enabling technology for microelectronic device manufacturing*, 2007 IEEE/SEMI Advanced Semiconductor Manufacturing Conference, June 11-12, 2007, Stresa, Italy; pp 291−297.

(11) Elam, J. W.; Zinovev, A.; Han, C. Y.; Wang, H. H.; Welp, U.; Hryn, J. N.; Pellin, M. J. Atomic layer deposition of palladium films on Al_2O_3 surfaces. *Thin Solid Films* **2006**, *515* (4), 1664–1673.

(12) Elam, J. W.; Zinovev, A. V.; Pellin, M. J.; Comstock, D. J.; Hersam, M. C. *Nucleation and growth of noble metals on oxide surfaces using atomic layer deposition*; The Electrochemical Society, Inc.: Pennington, NJ, 2007; Vol. 3, pp 271−278.

(13) Christensen, S. T.; Elam, J. W.; Lee, B.; Feng, Z.; Bedzyk, M. J.; Hersam, M. C. Nanoscale structure and morphology of Atomic layer deposition platinum on $SrTiO_3$ (001). *Chem. Mater.* **2009**, *21* (3), 516–521.

(14) Christensen, S. T.; Elam, J. W.; Rabuffetti, F. A.; Ma, Q.; Weigand, S. J.; Lee, B.; Seifert, S.; Stair, P. C.; Poeppelmeier, K. R.; Hersam, M. C.; Bedzyk, M. J. Controlled growth of platinum nanoparticles on strontium titanate nanocubes by atomic layer deposition. *Small* **2009**, *5* (6), 750–757.

(15) Setthapun, W.; Williams, W. D.; Kim, S. M.; Feng, H.; Elam, J. W.; Rabuffetti, F. A.; Poeppelmeier, K. R.; Stair, P. C.; Stach, E. A.; Ribeiro, F. H.; Miller, J. T.; Marshall, C. L. Genesis and evolution of surface species during Pt atomic layer deposition on oxide supports characterized by in-situ XAFS analysis and water-gas shift reaction. *J. Phys. Chem. C* **2010**, *114* (21), 9758–9771.

(16) Lashdaf, M.; Krause, A. O. I.; Lindblad, M.; Tiitta, A.; Venalainen, T. Behaviour of palladium and ruthenium catalysts on alumina and silica prepared by gas and liquid phase deposition in cinnamaldehyde hydrogenation. *Appl. Catal., A* **2003**, *241* (1−2), 65–75.

(17) King, J. S.; Wittstock, A.; Biener, J.; Kucheyev, S. O.; Wang, Y. M.; Baumann, T. F.; Gin, S. K.; Hamza, A. V.; Bauemer, M.; Bent, S. F. Ultralow lowading Pt nanocatalysts prepared by atomic layer deposition on carbon aerogels. *Nano Letters* **2008**, *8* (8), 2405−2409.

(18) Feng, H.; Elam, J. W.; Libera, J. A.; Setthapun, W.; Stair, P. C. Palladium catalysts synthesized by atomic layer deposition for methanol decomposition. *Chem. Mater.* **2010**, *22* (10), 3133–3142.

(19) Aaltonen, T.; Alen, P.; Ritala, M.; Leskela, M. Ruthenium thin films grown by atomic layer deposition. *Chem. Vap. Deposition* **2003**, *9* (1), 45–49.

(20) Aaltonen, T.; Ritala, M.; Sammelselg, V.; Leskela, M. Atomic layer deposition of iridium thin films. *J. Electrochem. Soc.* **2004**, *151* (8), G489–G492.

(21) Aaltonen, T.; Ritala, M.; Sajavaara, T.; Keinonen, J.; Leskela, M. Atomic layer deposition of platinum thin films. *Chem. Mater.* **2003**, *15* (9), 1924–1928.

(22) Aaltonen, T.; Ritala, M.; Leskela, M. ALD of rhodium thin films from $Rh(acac)_3$ and oxygen. *Electrochem. Solid-State Lett.* **2005**, *8* (8), C99–C101.

(23) Kim, S. K.; Lee, S. Y.; Lee, S. W.; Hwang, G. W.; Hwang, C. S.; Lee, J. W.; Jeong, J. Atomic layer deoposition of Ru thin films using 2,4-(Dimethylpentadienyl)(ethylcyclopentadienyl) Ru by a liquid injection sysytem. *J. Electrochem. Soc.* **2007**, *154* (2), D95.

(24) Christensen, S. T.; Elam, J. W. Atomic layer deposition of Ir-Pt alloy films. *Chem. Mater.* **2010**, *22* (8), 2517–2525.

(25) Jiang, X.; Gür, T. M.; Prinz, F. B.; Bent, S. F. Atomic layer deoposition (ALD) co-deposited Pt-Ru binary and Pt skin catalysts for concentrated methanol oxidation. *Chem. Mater.* **2010**, *22*, 3024–3032.

(26) Alayoglu, S.; Nilekar, A. U.; Mavrikakis, M.; Eichhorn, B. Ru-Pt core-shell nanoparticles for preferential oxidation of carbon monoxide in hydrogen. *Nat. Mater.* **2008**, *7* (4), 333–338.

(27) Kua, J.; Goddard, W. A. Oxidation of methanol and 2nd and 3rd row group VIII transition metals (Pt, Ir, Os, Pd, Rh, and Ru): Application to direct methanol fuel cells. *J. Am. Chem. Soc.* **1999**, *121* (47), 10928–10941.

(28) Carrette, L.; Friedrich, K. A.; Stimming, U. Fuel cells: Principles, types, fuels, and applications. *ChemPhysChem* **2000**, *1* (4), 162–193.

(29) Miller, J. T.; Kropf, A. J.; Zha, Y.; Regalbuto, J. R.; Delannoy, L.; Louis, C.; Bus, E.; van Bokhoven, J. A. The effect of gold particle size on the Au-Au bond distance and reactivity toward oxygen in supported catalysts. *J. Catal.* **2006**, *240*, 222–234.

(30) Elam, J. W.; Groner, M. D.; George, S. M. Viscous flow reactor with quartz crystal microbalance for thin film growth by atomic layer deposition. *Rev. Sci. Instrum.* **2002**, *73* (8), 2981–2987.

(31) Castagnola, N. B.; Kropf, A. J.; Marshall, C. L. Studies of Cu-ZSM-5 by X-ray absorption spectroscopy and its application for the oxidation of benzene to phenol by air. *Appl. Catal., A* **2005**, *290*, 110–122.

DOI: 10.1021/nl101567m | *Nano Lett.* **2010,** *10,* 3047–-3051